The Deep Space Atomic Clock: the first demonstration of a trapped ion atomic clock in space

E.A. Burt*, J.D. Prestage, R.L. Tjoelker, D.G. Enzer, D. Kuang, D.W. Murphy, D.E. Robison, J.M. Seubert, R.T. Wang, T.A. Ely
Jet Propulsion Laboratory, California Institute of Technology, Pasadena, CA‡

Abstract

Atomic clocks, which lock the frequency of an oscillator to the extremely stable quantized energy levels of atoms, are essential for navigation applications such as deep space exploration[1] and the Global Positioning System (GPS)[2] and as scientific tools for addressing questions in fundamental physics[3,4,5,6]. Atomic clocks that can be launched into space are an enabling technology for GPS, but to date have not been applied to deep space navigation and have seen only limited application to scientific questions due to performance constraints imposed by the rigors of space launch and operation[7]. The invention of methods to electromagnetically trap and cool ions has revolutionized atomic clock performance[8,9,10,11,12,13]. Terrestrial trapped ion clocks have achieved orders of magnitude improvements in performance over their predecessors and have become a key component in national metrology laboratories[13]. However, transporting this new technology into space has remained elusive. Here we show the results from the first-ever trapped ion atomic clock to operate in space. Launched in 2019, NASA's Deep Space Atomic Clock (DSAC) has operated for more than 12 months, demonstrating a short-term fractional frequency stability of between 1 and 2 x 10^{-13} at 1 second of averaging time (measured on the ground), a long-term stability of 3 x 10^{-15} at 23 days, and an estimated drift of 3.0(0.7) x 10^{-16} per day. Each of these exceeds current space clock performance by as much as an order of magnitude[14,15,16]. We found the DSAC clock to be particularly amenable to the space environment, having low sensitivities to variations in radiation, temperature, and magnetic fields, and we were able to characterize these in detail. This level of space clock performance will enable new types of space navigation. In particular, the DSAC mission has demonstrated a process called one-way navigation whereby signal delay times are measured in-situ making near-real-time deep space probe navigation possible[17].

Introduction

All space clocks in use today employ atomic beams or gas cells to confine atoms[14,15,16] . These clocks have short term stabilities ranging from 1 to 10 x $10^{-12}/\tau^{1/2}$ while long-term (greater than a day) stability, usually characterized by drift, is between 1 and 10 x 10^{-15}/day. Long-term clock autonomy, highly desirable for deep space and GNSS applications[18] is limited by drift usually due to interactions between atoms and vacuum chamber walls. Trapped ion clocks[19] solve this by

‡ The research was carried out at the Jet Propulsion Laboratory, California Institute of Technology, under a contract with the National Aeronautics and Space Administration (80NM0018D0004). Government sponsorship acknowledged. The technology demonstration mission was supported in part by the NASA Space Technology Mission Directorate (STMD) and in part by the NASA Space Communications and Navigation Directorate (SCAN). The authors are with the Jet Propulsion Laboratory, California Institute of Technology, Pasadena CA 91109 USA (e-mail: eric.a.burt@jpl.nasa.gov).

electromagnetically confining atoms, thereby completely eliminating wall collisions. Recently, a different type of beam clock was demonstrated in space with an inferred short-term stability of $3x10^{-13}/\tau^{1/2}$ [20], but no long-term stability was reported.

Because of the advantages to clock performance provided by atom trapping, virtually all primary atomic clocks used in national metrology labs employ some form of trapping[12,13] . Motivated by the low instability enabled by trapped ion clocks and by their potential to be very small, NASA's Jet Propulsion Laboratory (JPL) embarked on a series of mercury ion clock development projects aimed at ultimately producing a version that could be flown in space. Demonstrations in the laboratory achieved a stability of $2x10^{-14}/\tau^{1/2}$ [10] and drifts as low as $2.7x10^{-17}$/day[11]. While the approach followed at JPL used electromagnetic traps, it did not use lasers, cryogenics, or microwave cavities, enabling the technology to be robust, relatively small and to consume less than 50 W of power[10,23,24].

In 2011, with the success of these earlier ground-based demonstrations, NASA's Space Technology Mission Directorate started a project called the Deep Space Atomic Clock (DSAC) to demonstrate the first ever trapped ion atomic clock in space with the goal of $2x10^{-13}/\tau^{1/2}$ short-term stability and 3 x 10^{-15} stability at one day without the need to remove drift. This technology demonstration mission is designed to address the unique needs of deep space navigation[25], but given the clock's low size, weight, and power (SWaP), it is also well-suited for GNSS applications in Earth orbit. The DSAC payload, consisting of a trapped ion clock and its $1x10^{-13}$ class ultra-stable local oscillator (LO) together with a GPS receiver to facilitate comparisons with clocks on the ground, was launched into Earth orbit in June, 2019 (see Fig. 1) and first powered on in space in August, 2019. The two-year DSAC mission is designed to demonstrate clock operability, characterize performance of the technology in space, and to carry out several navigation experiments to demonstrate its utility in that domain.

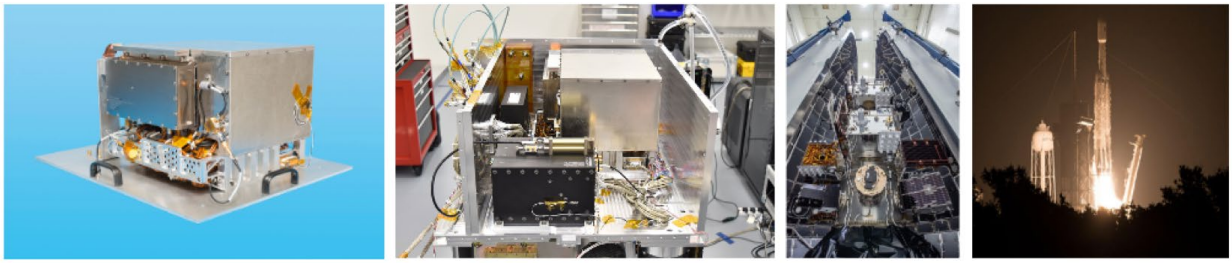

Figure 1. From left to right: The DSAC clock (credit JPL), the clock integrated in the spacecraft payload (credit General Atomics), the spacecraft being integrated into the launch vehicle (credit Space-X), and the launch of Space-X Falcon Heavy ST1 (credit NASA).

The DSAC trapped ion clock

The DSAC ion clock, payload configuration, and ground testing as well as its navigational uses and some scientific applications have been previously described[26,27]. Here, we summarize these and then focus on results obtained after launch.

At the heart of the DSAC clock are two linear RF Paul ion traps[28,29], one having 4 rods (the quadrupole or Load Trap – LT), the other having 16 rods (the Multi-pole – MP). Fig. 2 shows a

schematic cross section of the vacuum chamber revealing the traps. A radio-frequency voltage is applied across trap rod pairs with the field strength decreasing with distance away from the rods. Ions are displaced from high field values towards low, seeking the weakest field, which is in the center when viewed along the axis of the trap. The other two images in Fig. 2 show contour plots of field strength for the LT and MP in a plane perpendicular to this axis. In the LT, the non-zero time-average force on the ions from strong field to weak field regions gives rise to an effective quadratic potential proportional to E^2 where E is the electric field magnitude. Ions in the trapping region execute oscillatory motion at about 50 kHz in the radial direction (axially, ions are confined only by endcaps held at a DC voltage and move ballistically). The DSAC clock confines a cloud of up to 10^7 ions. The trapping force that pushes ions towards the center of the trap where the RF field is zero, is partially balanced by Coulomb repulsion pushing them outwards. As a result, the ion cloud occupies a region that extends radially about 1 mm such that the spatial- and ensemble-averaged RF field experienced by the trapped ions is non-zero. This region of confinement is smaller than the wavelength of microwave radiation used for interrogation so the first order Doppler shift, proportional to $-v/c$ (v is ion velocity and c is the speed of light), is eliminated[30]. However, while $\langle v \rangle = 0$, $\langle v^2 \rangle$ is not zero, so there is a small relativistic second order Doppler shift proportional to v^2/c^2. The main advantage of the MP trap, is that the radial potential created by this configuration approaches that of a square well as shown in the contour plot on the right side of Fig. 2. On average, ions in the MP experience a lower trapping field amplitude than in the LT, hence virtually eliminating this primary systematic effect in the clock[29].

The difference in quantized energy levels in an atom can serve as a stable frequency reference. To make a clock based on such a reference, a synthesized frequency referenced to a LO is used to interrogate the atoms or ions (see Fig. 3). In the case of Hg^+ used in DSAC, this is 40.5 GHz driving the $S_{1/2}$, F=0, $m_F = 0$ to $S_{1/2}$, F=1, $m_F = 0$ magnetic field insensitive hyperfine clock transition (see the Methods section for an energy level diagram). If the multiplied LO frequency is correct, the atomic response ("signal") will be large, otherwise it will be small. This response is used to form a correction that is fed back to the LO thereby closing the loop and transferring the atomic energy level stability to the output of the LO (DSAC actually uses a more complex LO architecture[31]. In DSAC a plasma discharge light source at 194 nm is used to prepare the initial state of the ions and to read out the state after microwave interrogation.

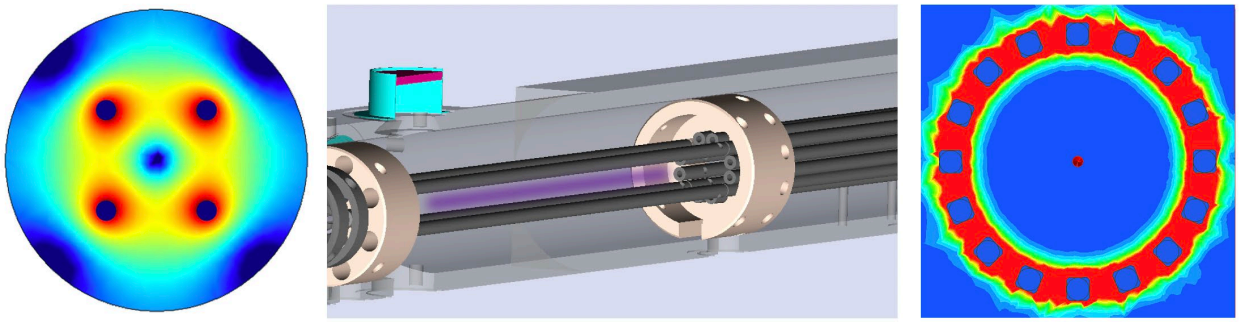

Figure 2. The center image is a cross section schematic of a DSAC-like vacuum chamber (light gray) showing the trap rods for the LT on the left and for the MP on the right (dark gray), the optical window assemblies (cyan and magenta), and a representation of the trapped ion cloud lying on the LT axis (purple). The image on the left shows a contour plot of the quadrupole trap RF amplitude in a plane perpendicular to the rods. Dark blue corresponds to low field and red to high field. The 4 symmetric blue circles correspond to the trap rods. The blue circle in the center is the low field region where the ions are trapped. The image on the right shows a contour plot of the multi-pole trap RF amplitude with the same color designations. Note that the center trapping

region in the multi-pole trap (dark blue) corresponds to a significantly larger fraction of the volume inside the trap rods than for that of the LT.

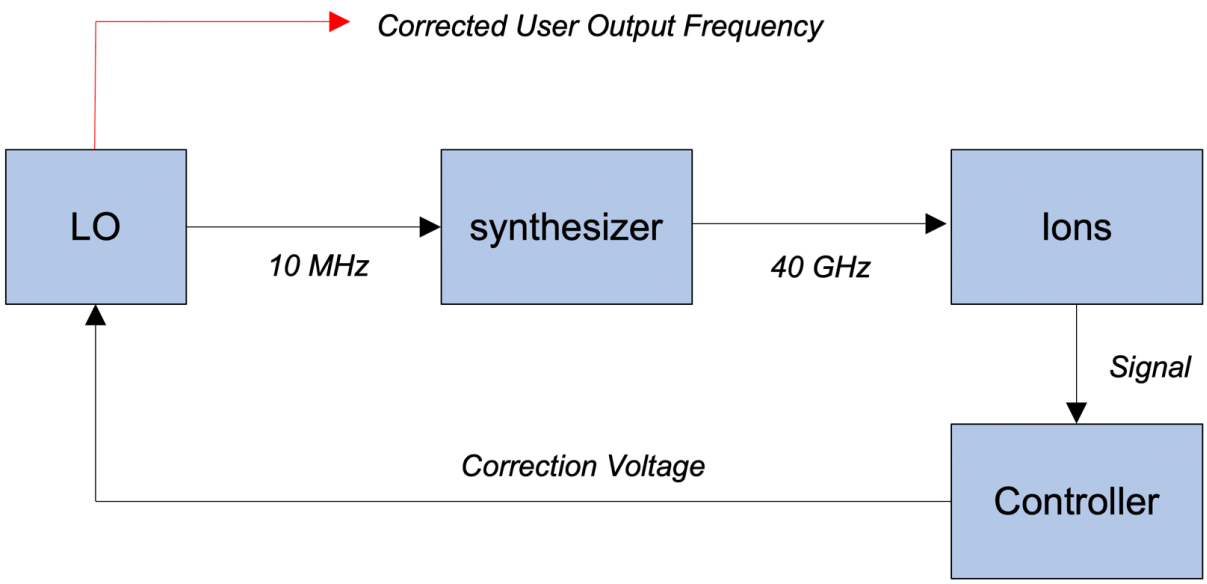

Figure 3. A simplified block diagram of the clock. The ultra-stable Local Oscillator or LO is a mechanical oscillator such as a quartz crystal, used as a reference for a synthesizer, which generates the 40.5 GHz ion resonance interrogation frequency. Ion measurements described in the text determine the error in this frequency and feed this back as a correction to either the LO or a user output synthesizer[31]. In this way the user output frequency is locked to the ion resonance.

Trapped ions are kept near room temperature via collisions with a neon buffer gas so that thermal excitations don't eject them from the trap. During DSAC clock testing, a small neon depletion mechanism was discovered, which rendered clock operation in the MP trap no longer viable (see the Methods section). While operation in the LT was still possible, the quadrupole LT design in this version of the clock is not optimized for clock operation. As a result, neither the short-term, nor long-term stability in the LT will be as good as those made possible by the MP trap design, but long-term stability in the LT still proved to be better than required and LT-based clock operation has been the primary mission configuration.

Clock ground testing

On the ground, a 1/e ion trap lifetime of 14 days was first measured. Over time this has further improved as trace gasses in the vacuum chamber were pumped away. The long trap lifetime, currently 30 days, indicates that trace background gas partial pressures are very low. Background gas and magnetic inhomogeneity can both lead to clock decoherence. Collisions with excess background neutral mercury can lead to charge exchange and decohering phase randomization, while collisions with other background gas can cause frequency shifts[32,33] as well as decoherence if their partial pressures are high enough. In the rest frame of the ion executing oscillatory motion in the trap, a magnetic gradient will appear as an oscillating magnetic field that can drive decohering $\Delta m_F = \pm 1$ field Zeeman transitions. The clock transition line trace in Fig. 4 taken with a Rabi interrogation time of 4 s has no excess broadening or loss of Rabi sideband structure indicating no decoherence within the noise of the measurement.

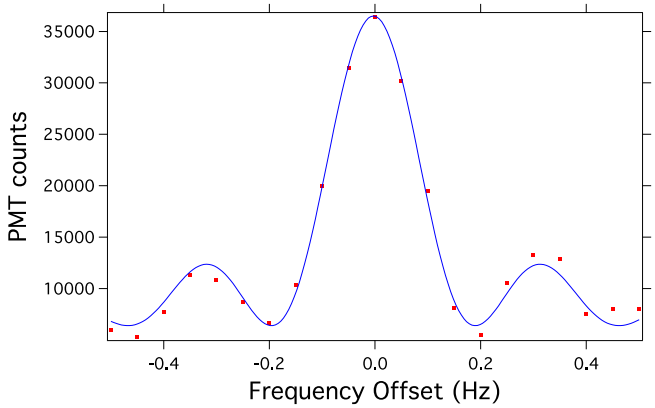

Fig. 4. The DSAC atomic line taken while operating in the MP trap with a Rabi interrogation time of 4 seconds.

Furthermore, by monitoring the signal contrast and frequency drift over time we can place a limit on the evolution of background gas to < $1x10^{-11}$ torr/day, a rate that can be sustained for years without deleterious effects.

On the ground, the DSAC clock demonstrated a stability of $2x10^{-13}/\tau^{1/2}$ operating in the MP with a maser as the LO (see Fig. 6). As reported previously[26], it also demonstrated a stability of $2x10^{-15}$ at one day.

Clock operation in space

Before running the clock continuously, it was thoroughly characterized in the space environment. The largest frequency shifts in the DSAC clock are due to magnetic, and ion number dependent relativistic Doppler, and background gas collision effects. Overall sensitivity to temperature changes, including electronic sensitivities, enter through these three fundamental paths. Here we only summarize these characterizations. See the Methods section for details on how each measurement was made.

Systematic Effects

During each orbit the magnetic field has a peak-to-peak variation of about 25 μT (250 milli-Gauss), over 100x more than in a typical laboratory setting. The combination of the low sensitivity of the Hg^+ clock transition to magnetic shifts (about 4x lower than cesium for example) and the three layers of magnetic shielding reduce associated frequency shifts to below the clock noise at the orbital period time. As verified above, variations in the clock frequency due to trace gas evolution are expected to be low due to the high-temperature bakeout applied during clock preparation. Measurements placed a limit on frequency variations due to this effect of well below 1 x 10^{-15} on a day time scale. As described above, first order Doppler effects are eliminated in this trap, but there are still residual relativistic second order Doppler effects in the LT. Among other things, these are dependent on the number of ions trapped, which is proportional to the clock signal size as observed through Photo-Multiplier Tube (PMT) counts. In experimental units the DSAC clock sensitivity was measured to be about -6 x 10^{-17}/count so that an ion number stability corresponding to 20 counts or 0.1% of the total is required to support clock stability at the 10^{-15} level. This level

of ion number stability is normally achieved after ion loading equilibrates with the residual trap loss mechanisms. The overall temperature sensitivity of the DSAC instrument is a combination of several factors, including relativistic Doppler effects, and stray temperature-dependent magnetic effects. When it was possible to disentangle these, the fundamental sensitivity of the clock was measured to be as low as -2.3(1.1) x 10^{-15}/°C *with no active thermal stabilization*. This point is particularly notable since rarely if ever are space clocks able to operate without some form of temperature control. Orbital transits through South Atlantic Anomaly expose the clock to a high radiation environment. This results in increased PMT counts and small changes in the LO frequency, but the DSAC control algorithm is designed to filter these out, so there is no observed impact on clock output (see the Methods section for details).

Clock Performance in Space

Performance in space in the repurposed LT with no temperature control

At clock start up, the LO frequency can be far off the correct value and it must be put on frequency before the clock can function normally – a process called LO acquisition[21]. An initial ion load gets the clock transition signal size close enough to run acquisition. Once the LO is acquired, the clock is allowed to reach thermal equilibrium. The DSAC vacuum chamber has a thermal time constant of about 4 hours, so 12 hours are usually required to fully stabilize temperature. During this time, the trapped ion number also slowly approaches its equilibrium value when operating the electron emitter (used to ionize neutral mercury) at its normal low power setting. The expected short-term performance for the clock operating in the repurposed LT is $8 \times 10^{-13}/\sqrt{\tau}$, greater than the instability achieved in the optimized MP, but still below the flight measurement system noise for averaging times of less than a day. However, the measurement system does allow an upper bound to be placed on short-term clock performance, and for averaging times greater than a day it can be used to measure long-term clock performance directly[22].

Fig. 5 shows 52 days of continuous frequency offsets for the DSAC clock and the GPS measurement system as compared to Universal Coordinated Time (see the Methods section for details). Clock drift is estimated using a linear least-squares fit, which gives a slope of +3.0(0.7)x10^{-16}/day.

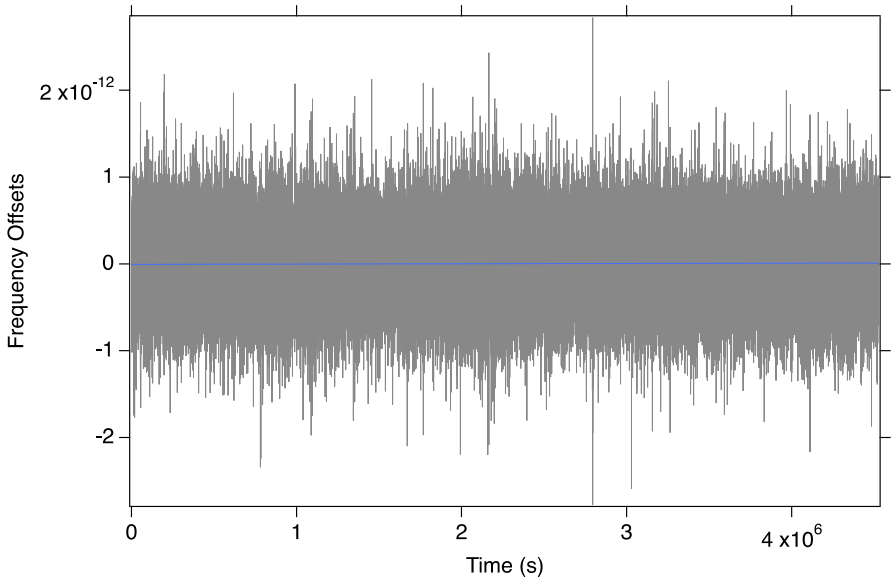

Figure 5. Frequency offsets of the DSAC instrument in LT mode operating in space vs. time (gray). The blue line is a least-squares fit to a straight line, which shows a drift of +3.0(0.7)x10^{-16}/day.

Fig. 6 shows the measured Allan deviation[34] for the same run. The deviation from white frequency noise (proportional to $1/\sqrt{\tau}$) after 10^5 s is consistent with slow thermal effects related to variations in the host spacecraft orientation relative to the sun (see Methods). The flicker noise floor of the clock and measurement system is not known, so flicker noise may also contribute on these time scales. A frequency stability of $3\text{x}10^{-15}$ corresponding to a time deviation (TDEV) of less than 4 ns is shown at 23 days. Over many separate runs, the clock stability at one day varied between 3 and 5 x 10^{-15} depending on the temperature variations for a given run. In addition to being taken in the lower-performing LT, this performance level is even more notable because the data were taken with the temperature control servo loop turned off during a time when the baseplate temperature varied by 9 °C. It is important to note that the noise floor of long baseline GPS time transfer measurements is near this level. Thus, the measurements stated here contain both clock and measurement system noise and so are an upper bound for the clock alone[11]. It is possible that GPS time transfer noise can average to lower values when one of the clocks being compared is in space because atmospheric effects are partially eliminated, but this has not yet been demonstrated. See the Methods section for details on the measurement system and GPS. This long-term performance, already more than 1 order of magnitude better than existing space clocks, will enable one-way navigation, allowing control of deep space satellites in near real-time [ref_DSACNavExp] as well as new planetary science measurements[17].

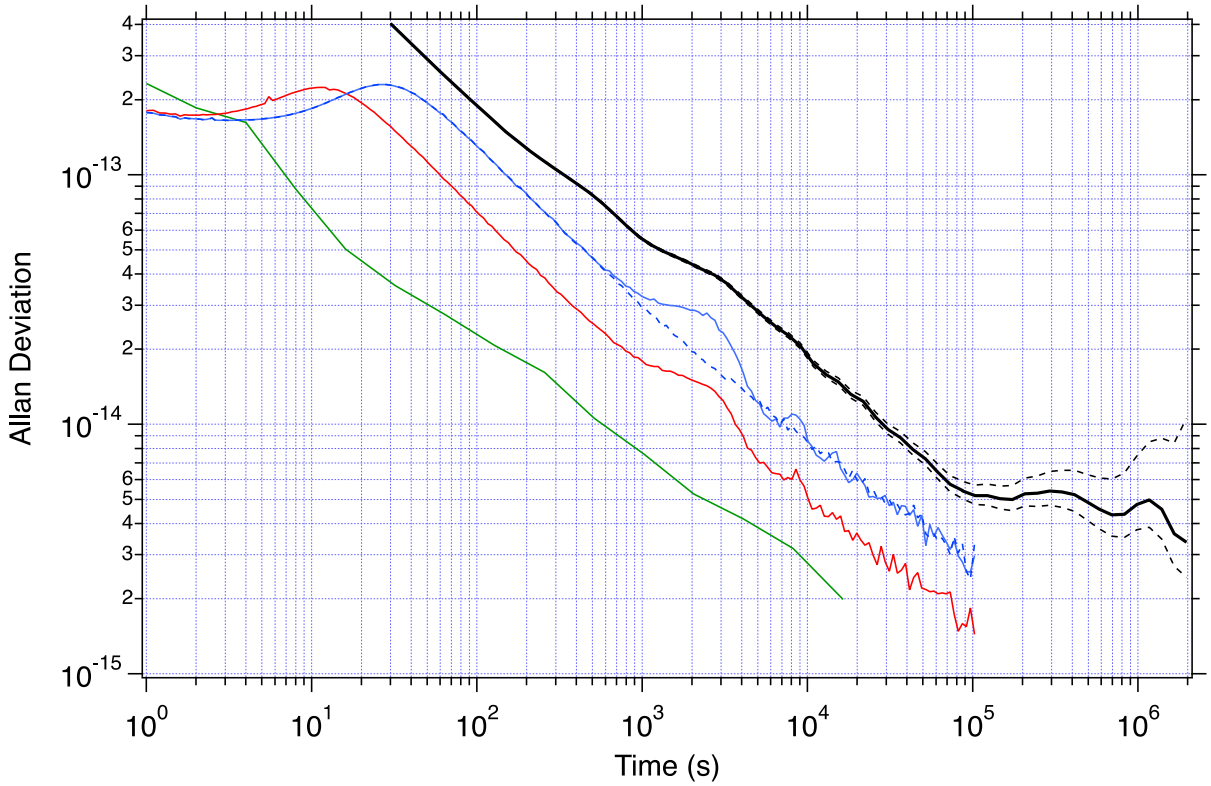

Figure 6. Allan deviation of the DSAC clock and GPS time transfer system compared to UTC while operating in the repurposed LT in space (solid black, dashed black lines indicate 68% confidence intervals). Temperature servo loops are disabled. Also shown is a simulation of expected clock performance with environmental disturbances at the orbital period (solid blue) and without (dashed blue). Clock operation parameters used here were not fully optimized. A simulation of expected clock performance with more optimal parameters is shown in red. The green trace shows operation achieved on the ground with the optimized MP trap and an H-maser acting as the LO. Note that the black trace is an overlapping Allan deviation, while all other traces are non-overlapping.

Conclusions

We have demonstrated the world's first trapped ion atomic clock operating in space. Clock operation was fully characterized over a 9-month period and long-term operation will continue through the remainder of the 2-year mission. On the ground, the clock's short-term stability measured in the multi-pole trap of the two-trap system was between 1 and 2×10^{-13} at one second and $2\times10^{-13}/\tau^{1/2}$, while in space the short-term stability in the repurposed load trap was $8\times10^{-13}/\tau^{1/2}$. In space a stability of between 3 and 5 x 10^{-15} was measured at one day and 3×10^{-15} was measured at 23 days, equivalent to a time deviation of less than 4 ns. In addition, an uncorrected drift rate of $+3.0(0.7)\times10^{-16}$/day was also observed, demonstrating this technology's utility for applications requiring autonomous operation. Both long-term observations were made in the presence of a 9 °C variation in temperature and with temperature control turned off. With clock sensitivities to environmental effects measured on the ground, operation in the more extreme environment of space was observed. In all cases, clock frequency shifts due to orbital environmental effects were near or below the noise floor of the measurement system and that of the estimated Allan deviation of the clock itself. Radiation effects due to orbital passes through the South Atlantic Anomaly were also studied and found to not limit clock operation. Follow-on work is already in progress

to extend the life time of this technology past the current expected 3 to 5 years, out to 10 years or more. These efforts will be focused on the UV light source and the vacuum chamber pressure, including the buffer gas and mercury vapor partial pressures. Infusion of this technology into future space flight missions is currently being explored with likely applications to one-way navigation and planetary science.

Acknowledgements

This work is jointly funded by NASA's Science, Technology, and Mission Directorate office and the office of Science, Communications, and Navigation.

Methods

Clock Operation Sequence

Fig. M1 shows a system level block diagram of the DSAC payload. A $1x10^{-13}$ class Ultra-Stable Oscillator (USO) serves as the LO providing 10 MHz to the DSAC 40.5 GHz synthesizer that generates the clock frequency and to a User Output synthesizer at 20.456 MHz used as the reference for the GPS receiver. The 40.5 GHz microwave signal is directed to the ion system to interrogate the trapped ions. The trap is enclosed in an ultra-high vacuum (UHV) system that is surrounded by 3 mu-metal magnetic shields. Also attached to the ion subsystem is the UV light subsystem, which consists of the plasma discharge lamp UV light source, optics, and a PMT detector. The detected signal is directed to the clock controller where software determines each frequency correction to be applied to the 40.5 GHz clock synthesizer and the user output synthesizer.

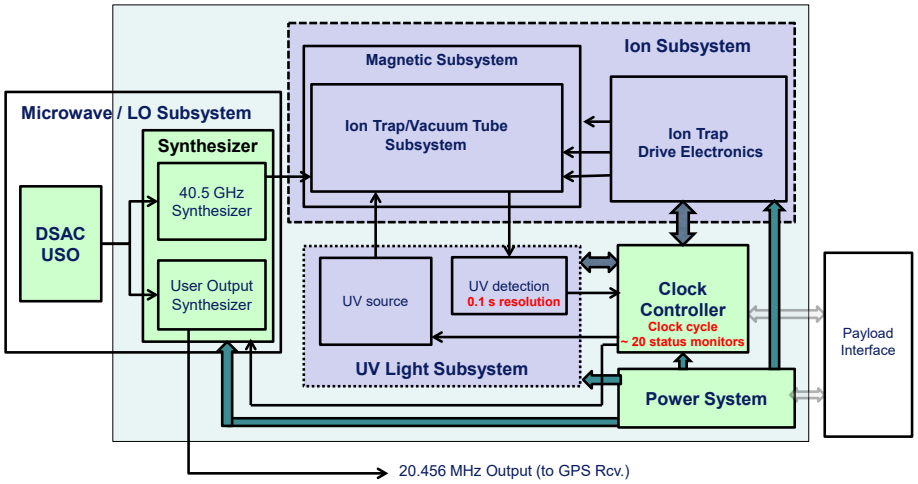

Figure M1. System-level block diagram of the DSAC payload. The GPS receiver is not shown.

The ultra-high vacuum (UHV) chamber includes a quadrupole "Load Trap" (LT) where ions are loaded and prepared, and a multi-pole trap (MP) where atom interrogation is performed. The DSAC clock also allows for atom interrogation and full clock operation to take place in the LT, though at a reduced performance level. Ions are loaded into the trap from a background neutral mercury vapor ionized by electrons from a heated LaB_6 filament held at a negative high voltage relative to the trap region. Clock electronics include RF drivers for the two traps, an electron

emitter driver, the clock controller, and a stable current source that drives coils surrounding the vacuum chamber to establish the clock quantization axis. The UV light source is enclosed in a hermetically sealed O_2 back-filled cell. DC bias fields are applied to the LT and MP trap rods to affect transfer ("shuttling") of ions between the two traps. All telemetry, including clock signal counts, background counts, frequency corrections, and many temperatures, are relayed to the ground on a daily basis.

Atomic Energy Level Diagram

Fig. M2 shows the ^{199}HgII level structure along with the various transitions used in the clock. The $S_{1/2}$, F=0, $m_F = 0$ to $S_{1/2}$, F=1, $m_F = 0$ field-insensitive hyperfine transition forms the basis of the clock. It is optimally driven by a microwave field at 40.5 GHz polarized parallel to the quantization axis. In DSAC, the microwave launcher establishes a field that is at 45º relative to this axis so it has a component both perpendicular and parallel. The perpendicular component can be used to drive the magnetically sensitive neighboring lines for diagnostic purposes. The $S_{1/2}$, F=1 to $P_{1/2}$, F=1 optical transition is driven by a plasma discharge source at 194 nm and is used to optically pump ions into the initial state and to read out the state after microwave interrogation.

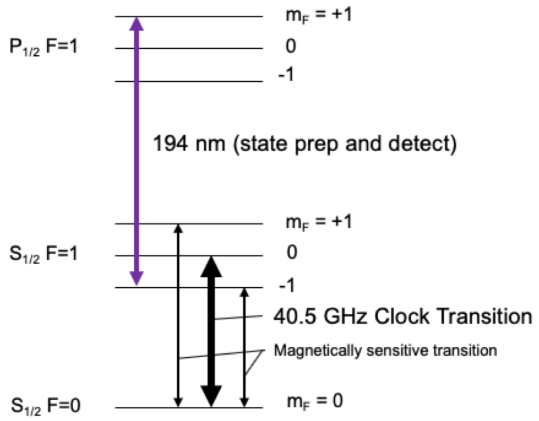

Figure M2. Level diagram for ^{199}HgII showing the $S_{1/2}$, F=1 to $P_{1/2}$, F=1 optical electric dipole transition used for state preparation and read out (purple), the $S_{1/2}$, F=0, $m_F = 0$ to $S_{1/2}$, F=1, $m_F = 0$ magnetic field insensitive 40.5 GHz hyperfine clock transition, and the $\Delta m_F = \pm 1$ field sensitive Zeeman lines.

The stability measurement system – GPS

Measurement noise floor, limitations

It is possible to determine most of the clock performance characteristics from its own telemetry. For instance, with a knowledge of the Signal-to-Noise Ratio (SNR) and atomic line Q of the clock transition, along with clock operation parameters, one can determine its short-term stability directly using:

$$\sigma_y(\tau) = \frac{1}{\pi\, SNR_{1/2}\, Q} \sqrt{\frac{t_c}{\tau}} \qquad (1)$$

Where τ is the averaging time, t_c is the clock cycle time, $SNR_{1/2}$ is the signal-to-noise ratio at the at the half-height of the resonance line, and $Q = f_0/\Delta f$ where f_0 is the ion resonance frequency and Δf is the Full Width at Half Maximum (FWHM) of the resonance line shape. $SNR_{1/2}$ is easily estimated using the periodically measured resonance signal size and by assuming shot-noise limited performance on the detection system. The Q is determined by the known resonance frequency and the interrogation time (Rabi time), which determines the FWHM. In the repurposed LT used for the space demonstration, with t_c = 12.5 s, f_0 = 40.5 GHz, $SNR_{1/2}$ = 19, and a Rabi interrogation time of 2 s, the estimated short-term stability is $8\text{x}10^{-13}/\tau^{1/2}$ (including aliasing noise[35]). However, to determine the clock's long-term stability requires a comparison to a second clock that is more stable on the time-scale of interest. Rather than carry a second clock on board the space craft, the DSAC project included a Global Positioning System (GPS) receiver. This enables GPS carrier phase time transfer[36], or comparison, to any clock on the ground also connected to a GPS receiver, in particular, UTC (Coordinated Universal Time). In principle, this enables comparison to the most stable clocks in the world since all national metrology laboratories use this method. However, this measurement technique is not without limitations: it is noisy in the short term and does not consistently average below a fractional frequency noise floor of 10^{-15} for long-baseline comparisons[11]. For averaging times where the noise of the DSAC clock is below the measurement noise floor, it is only possible to place an upper bound on clock stability performance at this time.

To perform the clock comparison, the GPS receiver must be carefully configured for operation in space. In particular, for the DSAC mission, it was necessary to calibrate the carrier phase and pseudo-range measurements for the receiver's temperature sensitivity. In addition, DSAC telemetry must be corrected for relativistic variations: the gravitational red shift and Doppler shifts. To facilitate each comparison, the receiver is dynamically transformed to the geoid[37] using the following equation:

$$\tau_s = \int dt \left[1 + \frac{\Phi(r) - \Phi_0}{c^2} - \frac{v^2}{2c^2}\right] \tag{2}$$

where τ_s is the space craft proper time, $\Phi(r)$ is the Newtonian gravitational potential at radius r from the geoid, Φ_0 is the gravitational potential on the Earth's geoid, c is the speed of light, and v is the speed of the space craft in the Earth-Centered Inertial reference frame (ECI).

Furthermore, in order to obtain accurate solutions, the second order terms in a multi-pole expansion of the gravitational potential must be retained so that,

$$\Phi(r) = -\frac{GM}{r}\left[1 - J_2\left(\frac{a_1}{r}\right)^2 \frac{(3z^2 - r^2)}{2r^2}\right] \tag{3}$$

where J_2 parameterizes the quadrupole contribution to the gravitational potential, a_1 is the equatorial radius of the Earth, and z is the third Cartesian component of the position vector $\boldsymbol{r}$. Without the additional J_2 terms in the potential, clock comparisons to the ground are limited by GPS errors. This was also demonstrated on the GRACE satellites as described in[37].

A careful analysis of expected DSAC measurement system noise was carried out in[22] that characterized the impact of the known, significant error sources. The most significant of these include: GPS measurement noise, GPS orbit and clock estimate errors, multipath errors, ground reference clock instabilities, and GPS receiver phase thermal calibration errors. Also included, but not as significant, were uncertainties with modeling spacecraft drag accelerations, spacecraft solar pressure accelerations, and the phase center knowledge of the GPS antenna with respect to the spacecraft center of mass. Fig. M3 shows the measured overlapping Allan deviation with and without corrections for relativistic and GPS receiver thermal effects. Superimposed is also the simulated expected clock performance up to a day of averaging with the clock parameters used during the run with and without effects from orbital thermal and magnetic disturbances.

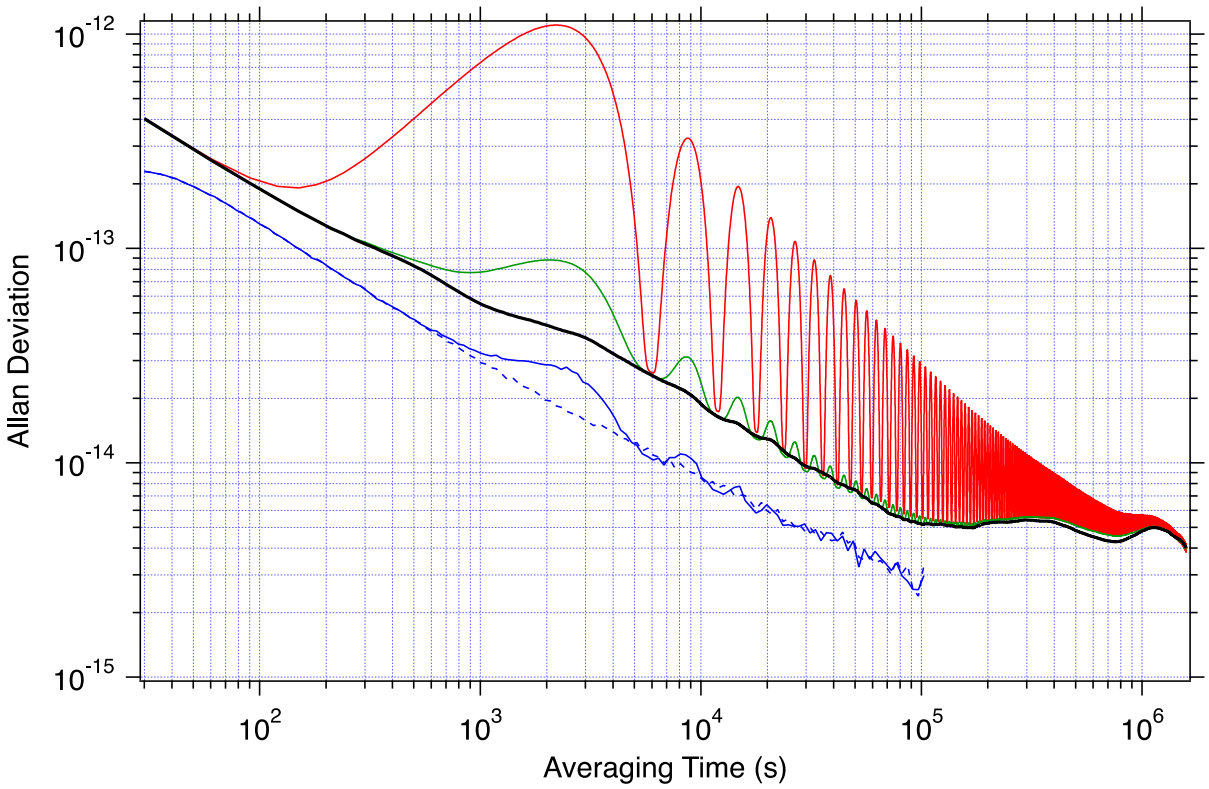

Figure M3. Measured Allan deviation without any corrections (red), with relativity corrections, but no temperature corrections (green) and with both relativity and temperature corrections (black). Simulated expected clock performance with clock parameters during the run is show in blue. All traces except the blue are overlapping Allan deviation.

The resultant effect of the measurement system errors is to yield an upper bound estimate of the clock's performance, and it is only for averaging times greater than a day that the measured Allan deviation begins to show clock performance.

Magnetic Effects

An environmental aspect that must be managed by most space clocks is variations in the ambient magnetic field. The quantization axis of the DSAC clock is determined by a coil inside the magnetic shields and a stable current source that generates a field of about 100 mG. The stability of this current source is at the 10 ppm level resulting in random field variations of 1 uG and clock

variations due to this internal current source noise well under 10^{-15}. Sensitivity to external magnetic variations is reduced by 3-layer mu-metal shielding. The sensitivity due to external magnetic field variations in the weakest shielding direction around the LT was measured on the ground to be $7x10^{-14}$/G. (The sensitivity in the optimized MP trap region is over an order of magnitude smaller.)

At the DSAC orbit of approximately 720 km, the clock sees variations in Earth's magnetic field of 250 mG, a range that is over 100x the variations that are typically seen in the laboratory. There are three mitigating factors that reduce the effects of these large magnetic field variations for the DSAC clock: 1) at an atomic response of 97 μHz/mG^2, the mercury clock transition has a very low sensitivity to magnetic variations (about 4x less than cesium, for example); 2) the use of high-performance magnetic shielding with a shielding effectiveness of up to 20,000 (though not as good in the LT); and 3) the variations occur at the orbital period of about 6000 seconds at which time their contribution to the clock Allan deviation is below the noise floor of the clock. Fig. M4 shows magnetic field amplitude variations as a function of time near the clock as measured by a magnetometer on the space craft. Fig. M5 shows the simulated Allan deviation of frequency shifts calculated in the worst case (weakest shielding direction always aligned with maximum field direction) from the measured field variations. Superimposed is the expected DSAC clock noise floor for operation in the MP without LO aliasing effects[35] ($2x10^{-13}/\tau^{1/2}$) and for the LT ($8x10^{-13}/\tau^{1/2}$). For both modes of operation, the magnetic effect (assuming the worst-case magnetic shielding direction) is just at, or is below the noise floor.

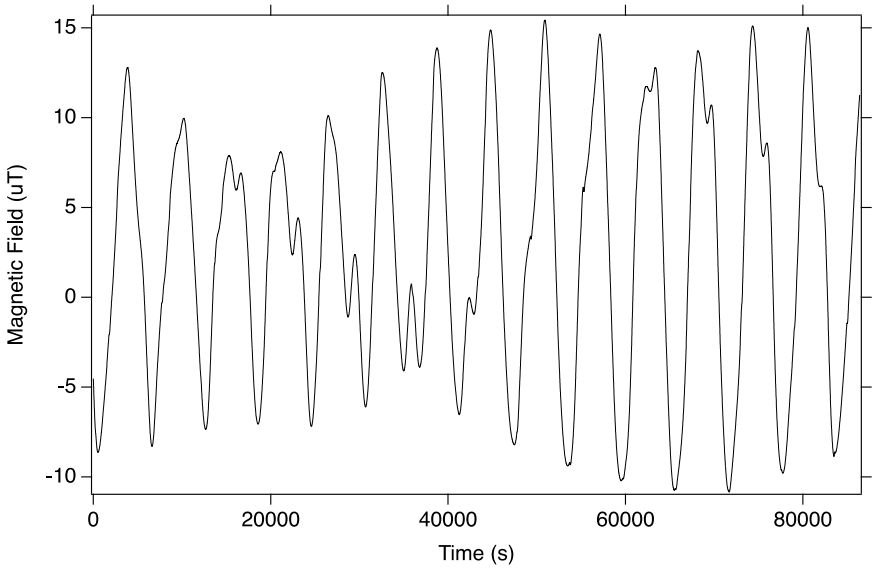

Figure M4. Variations in the magnitude of Earth's magnetic field observed on the DSAC space craft as a function of time. The orbital period is approximately 6000 seconds at 720 km.

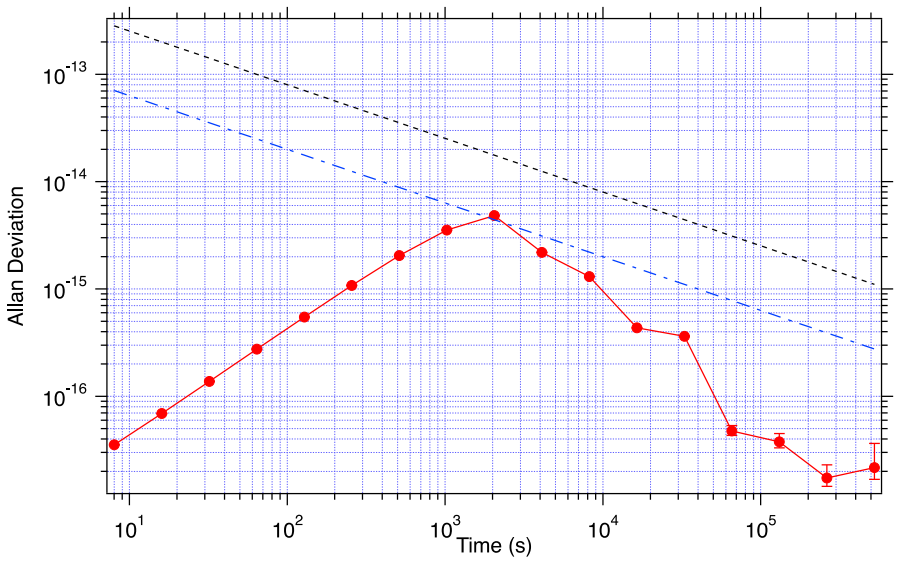

Figure M5. Allan deviation of the frequency shift associated with measured magnetic field variations on board the DSAC space craft (red) assuming a worst-case $7x10^{-14}$/Gauss sensitivity. Reference lines are also shown for expected MP (dashed blue) and LT (dashed black) operation noise floors (without LO noise aliasing effects for the MP line).

Thermal and Doppler Effects

During pre-launch evaluations it's usually possible to vary one parameter while holding others constant. In space this is rarely possible. The overall thermal sensitivity of the clock and the sensitivity to variations in the number of ions trapped – the number-dependent second order Doppler effect $df/f = -v^2/2c^2$ – are an example of effects that are difficult to decouple. For the latter, as the ion cloud changes size the time-averaged trap rf field amplitude as seen by the ions varies leading to changes in the ensemble-averaged ion velocity v and the second order Doppler shift[38]. Over a particular 4-day period, the clock temperature varied by about 5 ºC and the number of trapped ions was intentionally varied by about 50% with the electron emitter turned off. The frequency shift coefficients due to these are easily separated by exploiting the different functional forms of their variation (one was monotonic while the other was not). With the large change in trapped ion number here, the change in the associated second order Doppler effect dominates temperature related effects. The trapped ion number is not known directly, but is approximately proportional to clock signal size. Fig. M6 shows a least-squares second-order polynomial fit of frequency offsets plotted against signals size.

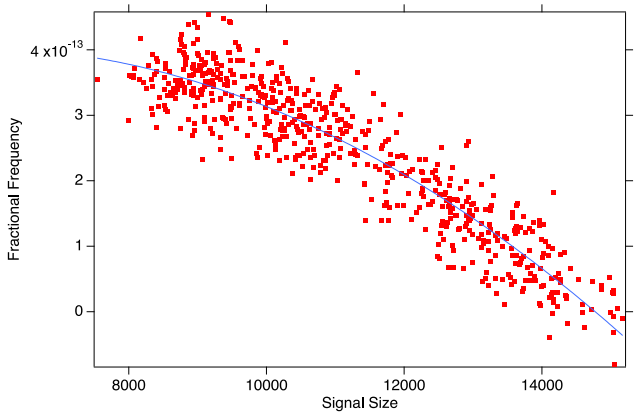

Figure M6. Frequency vs. signal size in the load trap. The slope gives an estimate of the number-dependent second order Doppler shift while operating in the LT.

Theoretically the dependence should be linear and the deviation from linearity at higher signal sizes shown is due to larger ion clouds extending beyond the optical interrogation region. Larger ion clouds are also subject to additional RF heating. Thus, the linear component of the fit, effectively extrapolating back to an empty trap, gives the most reliable representation of the second order Doppler shift coefficient. In experimental units this is $-5.6(1.2)\times10^{-17}$/count. For a current clock signal of 23,000 counts this corresponds to a total effect of about -1×10^{-12} for a full trap. To maintain 1×10^{-15} stability at a day requires constraining the trapped ion number to a fraction of a percent.

The residuals to the polynomial fit used to obtain the Doppler sensitivity have a systematic trend correlated with the variation in temperature, which was not monotonic. When the residuals are plotted against the temperature, a linear trend is apparent (see Fig. M7). The linear slope gives the temperature sensitivity in this case of $-2.3(1.1)\times10^{-15}$/°C. This is close to the thermal Doppler limit[39] and demonstrates how this technology is able to achieve a high level of stability in a varying thermal environment, even with no temperature control.

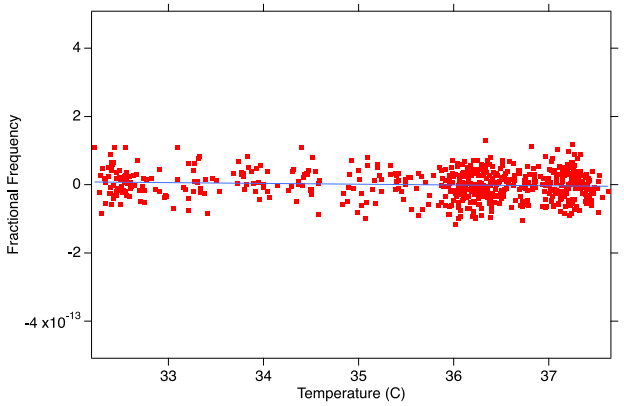

Figure M7. Residuals from a fit to frequency vs. signal size, now plotted against temperature in the LT. A linear fit gives a temperature sensitivity of $-2.3(1.1)\times10^{-15}$/C

The most important thermal variations occur at the orbital period of 6000 s, but there are other thermal time scales as well. For instance, on a roughly daily cadence the orbital ground track passes over regions that have different albedos, such as the Sahara Desert. Another temperature variation at an approximate daily period is certain spacecraft housekeeping activities. These can require an increase in spacecraft power consumption, which leads to variations in the spacecraft temperature. Finally, the solar illumination of the spacecraft varies on a roughly month time scale as the solar elevation angle, or beta angle, with respect to the orbital plan changes (The beta angle is defined as the angle between a line from the earth to the sun and the orbital plane.) This combined with occasional spacecraft re-orientations to keep the main spacecraft radiator in shadow lead to an approximate 17-day period in the temperature as seen by the ions in this data set. Fig. M8 shows the temperature in the LT, the most relevant temperature for current clock operation, as a function of time.

The DSAC demonstration mission currently operates with no thermal control. The instrument internal temperature floats with the changing environment and lags with a several hour time constant. Fig. M8a shows 52 days of data and an overall approximately periodic temperature trend associated with the variation in the space craft beta angle. The average peak-to-peak variation is about 4 °C with an average period of about 17 days. Fig. M8b is a 5-day subset and shows an approximate daily sinusoid in temperature with a peak-to-peak variation of 0.5 °C. Finally, fig. M8c is a 1-day subset showing the orbital effect with a peak-to-peak variation of about 0.3 °C. The overall temperature sensitivity of the measurement is due to a combination of several factors, not all of which are constant over time nor fundamental to the technology. In addition to the ions themselves, these effects include temperature sensitivities of the synthesizer, GPS receiver, and USO. In the data set shown in Fig. M8, the average measured temperature sensitivity was about 1.3×10^{-15}/°C. Coupled with the measured temperature variations, this sensitivity is not able to explain the peaks in the Allan Deviation curve at either ~3×10^5 s or ~1×10^6 s or the general flattening above 1×10^5 s. However, a more detailed analysis accounting for variations in the temperature sensitivity, overall drift, and other noise sources can explain these features. The one-day sinusoidal temperature variation coupled with this sensitivity would result in an Allan deviation peak of 0.36 x 0.5°C x 1.3×10^{-15}/°C ~ 2×10^{-16} occuring at 0.37 x 1 day ~ 3 x 10^4 s[31]. Similarly, the orbital variation would cause a peak of ~1e-16 occuring at 2200 s. Both are below the noise floor of the measurement. The small orbital peak in the measured Allan deviation in Fig. M3 and in the main text (see Fig. 5 there) is consistent with a peak in the simulated results shown in those figures. The simulation is based on measured sensitivities and measured orbital disturbance sizes. The resultant peak is dominated by USO temperature sensitivity with some contribution from a differential synthesizer phase temperature sensitivity, which only manifests itself as a frequency shift when the temperature has a non-zero time derivative[31]. The USO is discussed in more detail below. The simulated Allan deviation in Fig. M3 includes all known orbital clock disturbances (ions, synthesizers, and USO, but not GPS) and shows that these disturbances are expected to be near or below the estimated noise floor.

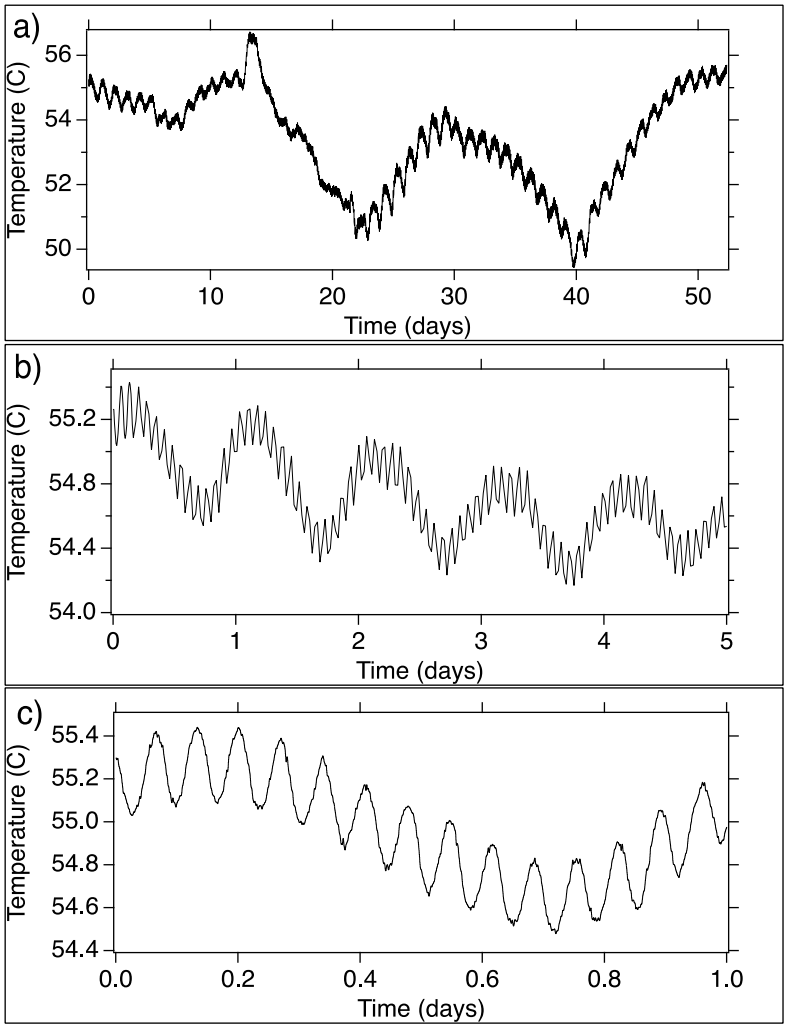

Figure M8. Temperature data shown for the 52-day data set described in the main article: (a) long-term temperature variation in the LT over 52 days correlated with the sun beta angle changes. (b) A 5-day subset showing 24-hour temperature variations. (c) A 1-day subset showing orbital temperature variation.

Pressure evolution

Background gas collision frequency shifts generally don't limit clock operation if the vacuum chamber is properly prepared[40]. In the getter-pumped DSAC clock the evolution of the CH_4 and H_2 partial pressures due to outgassing is measured on the ground to be well below $1x10^{-10}$ torr/day. H_2 is efficiently pumped by the in-situ getter with a very high pumping speed, but CH_4 is only weakly interacting and pumped very slowly by "cracking" into C and H_2 (both readily pumped) by a hot filament[41]. Due to the high H_2 pumping speed, its partial pressure is likely to be very stable in the long term (> 1 day). However, given the weak pumping speed of CH_4 it is possible that this could have a long-term evolution leading to a clock frequency drift. Here we place a limit on this variation. With a measured gas shift coefficient of $-3.5x10^{-5}$/torr for CH_4 [32,33], the corresponding frequency shift should be less than $3.5x10^{-15}$/day. Fig. M9 shows data taken when the trapped ion number was very stable (> 3 weeks after a power cycle, the clock frequency variations due to the number-dependent second order Doppler shift are < $3x10^{-16}$/d). The next dominant effect is due to temperature variations, which can be reliably distinguished from a linear

drift because the temperature has a turnover. The data are corrected for this measured temperature effect, and then fit to a straight line. The fitted slope is $2.7(5.3)\text{x}10^{-21}$/s, giving an upper bound on clock frequency variations due to trace gas evolution of $4.6\text{x}10^{-16}$/d, which improves on the upper bound on CH_4 pressure variation to $< 1.3\text{x}10^{-11}$torr/day[42]. This is also consistent with the low overall clock drift observed for the longest operational run (see Fig. 4 in the main text.)

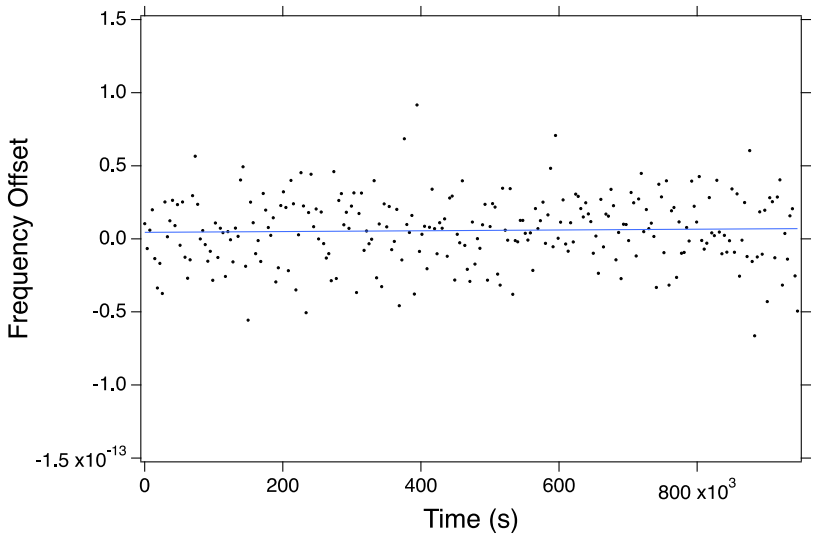

Figure M9. Frequency data with the temperature effect removed (black dots) and fit to a straight line (blue line) so as to place a limit on frequency shifts due to trace gas evolution in the clock vacuum chamber of $4.6\text{x}10^{-16}$/d.

USO Sensitivities

While the USO has its own temperature sensitivity, changes in the USO frequency due to temperature are by design, highly suppressed by the clock control loop. Linear USO drift could result in an offset on the clock output frequency, but has no effect on the clock Allan deviation. However, non-linear changes, such as a jump in the linear rate, or a sinusoidal variation with temperature will be present in both the output frequency and the Allan deviation. Since these effects can limit clock performance, a USO drift compensation algorithm[8] is built into the clock control loop that reduces the impact of sudden changes in linear USO drift (rare) by a factor of 4 to 5 when calculated for current operational parameters. Of biggest concern to DSAC are orbital variations in USO temperature, and the full control algorithm with drift compensation is calculated to reduce the impact of these by 0.017 for current operational parameters, enough to prevent the prominent $2.8\text{x}10^{-12}$ peak-to-peak USO orbital disturbance from impacting clock performance beyond the small residual (USO dominated) peak seen in the simulated curve of Fig. M3.

Radiation effects and the South Atlantic Anomaly

When the clock was first turned on in space one observation was how it responded to the radiation doses received when passing through the South Atlantic Anomaly (SAA)[43]. This radiation is primarily high energy protons with energies up to 100 MeV[44]. This radiation impacts PMT counts and USO drift rate, both at levels the control algorithm successfully mitigates.

Radiation-induced excess PMT counts is a well-established phenomenon and expected[45]. What is not as well-known is the quantitative response of a particular PMT to a given radiation environment and how it might impact the clock output. Fig. M10 shows excess photon counts as a function of time during passes through the SAA. The maximum radiation count rate shown is about 37,500 counts, including a maximum slope of about 80 counts/s, for these 8.1 s count intervals. The data shown is taken when the UV light source is in a low-level state where background light contributes only about 6000 counts each second, making the SAA effect clearer. When the UV light source is in its bright state for atomic state read out, the background counts due to scattered UV light are about 60,000 counts each second. For the bright state's 3.5 second clock read out time, the SAA therefore supplies at most 16,200 radiation counts with a maximum change of 35 counts/s. PMT counts are the only clock observable and one might think that varying PMT counts would appear to the clock algorithm as a frequency shift. The slope at half-height on the clock transition line is about 84,000 counts/Hz, so a 35 counts/s radiation induced excess could be interpreted as a 0.4 mHz or 10^{-14} fractional frequency shift per second. Fortunately, the control algorithm is first order insensitive to lamp brightness changes due to windowing that compares the brightness on alternating sides of the resonance over the previous three cycles[31]. Higher order impact is ruled out through modeling and through the lack of unexplained orbital peaks on the clock output Allan deviation.

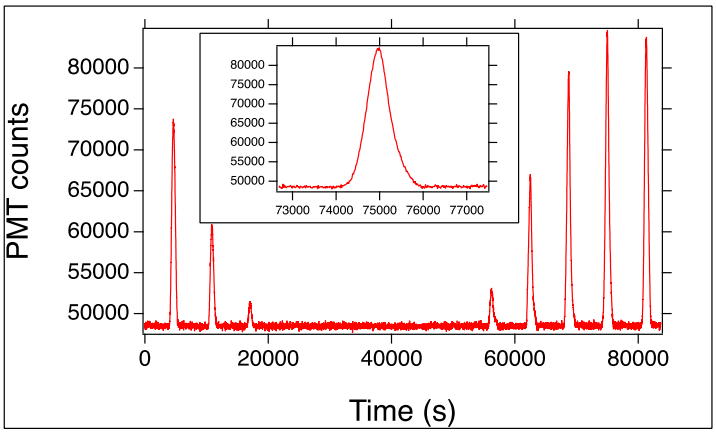

Figure M10. Total PMT counts in 8.1 second portions of each clock cycle as a function of time showing excess counts due to passage through the SAA. Each passage is approximately 20 minutes as shown for the expanded view inset. The varying peak amplitude is due to space craft orbital precession, which varies the trajectory of the space craft in and out of the SAA on a daily time scale.

The other observed impact of SAA transits has been on the USO drift rate. The accumulated USO response to radiation is slower, so explicit orbital variations are not resolved. Instead, a slow diurnal-like variation on the USO drift rate is observed. For the half-day that SAA passes occur, the USO has a higher drift rate than for the half-day that SAA passes do not occur. These two rates are very repeatable from one day to the next, resulting in a diurnal-like sinusoidal modulation on top of the average drift rate. This large 10^{-11} scale disturbance is filtered by the control algorithm to a level below the clock noise floor, largely because of its slow nature.

References

1. C. L. Thornton, J. S. Border, John Wiley & Sons., and Wiley InterScience (Online service), Radiometric tracking techniques for deep-space navigation. Wiley-Interscience, 2003.

2. L. A. Mallette, J. White and P. Rochat, "Space qualified frequency sources (clocks) for current and future GNSS applications," *IEEE/ION Position, Location and Navigation Symposium*, Indian Wells, CA, 2010, pp. 903-908.
3. J.D. Prestage, R.L. Tjoelker, and L. Maleki, "Atomic clocks and variations of the fine structure constant," Phys. Rev. Lett. 74, 3511 (1995)
4. Safronova, M. S., "The Search for Variation of Fundamental Constants with Clocks," *ANNALEN DER PHYSIK* 2019, 531, 1800364. https://doi.org/10.1002/andp.201800364
5. W.F. McGrew, X. Zhang, R. J. Fasano, S. A. Schäffer, K. Beloy, D. Nicolodi, R. C. Brown, N. Hinkley, G. Milani, M. Schioppo, T. H. Yoon, A. D. Ludlow, "Atomic clock performance enabling geodesy below the centimeter level," *Nature* 564, 87 (2018).
6. A. Hees, J. Guéna, M. Abrall, S. Bize, and P. Wolf, "Searching for an oscillating massive scalar field as a dark matter candidate using atomic hyperfine frequency comparisons," Phys. Rev. Lett. 117, 061301 (2016).
7. There are a few notable exceptions, for instance: R.F.C. Vessot; et al. (1980). "Test of Relativistic Gravitation with a Space-Borne Hydrogen Maser," Phys. Rev. Lett. 45 (26): 2081–2084
8. J.D. Prestage, G.J. Dick, and L. Maleki, "Linear ion trap based atomic frequency standard," IEEE Trans. Instrum. Meas. 40, 132 (1991).
9. L.S. Cutler, R.P. Giffard, and M.D. McGuire, "A trapped mercury 199 ion frequency standard," Proc. 13th Ann. Precise Time and Time Interval (PTTI), pp. 563-577 (1981)
10. R.L. Tjoelker, et al., "A mercury ion frequency standard engineering prototype for the NASA deep space network," Proc. Of the 50th annual IEEE International Frequency Control Symposium, pp. 1073-1081 (1996).
11. E.A. Burt, W.A. Diener, and R.L. Tjoelker, "A Compensated Multi-pole Linear Ion Trap Mercury Frequency Standard for Ultra-Stable Timekeeping," IEEE Trans. On Ultrasonics, Ferroelectrics, and Frequency Control 55, pp. 2586-2595 (2008).
12. N. Hinkley, J.A. Sherman, N.B. Phillips, M. Schioppo, N.D. Lemke, K. Beloy, M. Pizzocaro, C.W. Oates, A.D. Ludlow, "An atomic clock with 10^{-18} instability," Science 341, pp. 1215-1218 (2013)
13. S.M. Brewer, J.-S. Chen, A.M. Hankin, E.R. Clements, C.W. Chou, D.J. Wineland, D.B. Hume, and D.R. Leibrandt, "$^{27}Al^{+}$ Quantum-logic clock with a systematic uncertainty below 10^{-18}," Phys. Rev. Lett. 123, 033201 (2019)
14. R. Lutwak, D. Emmons, R.M. Garvey, and P. Vlitas, "Optically pumped cesium-beam frequency standard for GPS-III," Proc. 33rd Ann. Precise Time and Time Interval (PTTI), pp. 19-30 (2001).
15. W.J. Riley, "Rubidium atomic frequency standards for GPS block IIR," Proc. 22nd Ann. Precise Time and Time Interval (PTTI), pp. 221-230 (1990).
16. F. Droz *et al*., "Space Passive Hydrogen Maser - Performances and lifetime data," *2009 IEEE International Frequency Control Symposium Joint with the 22nd European Frequency and Time forum,* Besancon, 2009, pp. 393-398.
17. J. Seubert, T. Ely, and J. Stuart, "Results of the deep space atomic clock deep space navigation analog experiment," Proceedings of the AAS/AIAA Astrodynamics Specialist Conference, August 9-12, 2020 [page number awaiting publication].
18. A. Codik, "Autonomous navigation of GPS satellites: a challenge for the future," Journal of the institute of navigation 32, pp. 221-232 (1985).
19. H. G. Dehmelt, "Monoion oscillator as potential ultimate laser frequency standard," in *IEEE Transactions on Instrumentation and Measurement*, vol. IM-31, no. 2, pp. 83-87, June 1982
20. Liu, L., Lü, D., Chen, W. *et al.* In-orbit operation of an atomic clock based on laser-cooled ^{87}Rb atoms. *Nat Commun* **9,** 2760 (2018).
21. R.L. Tjoelker, E.A. Burt, S. Chung, R.L. Hamell, J.D. Prestage, B. Tucker, P. Cash, and R. Lutwak, "Mercury atomic frequency standards for space-based navigation and timekeeping," Proc. of the 43rd annual Precise Time and Time Interval Systems and Applications Meeting, pp. 209-304 (2011).
22. T. A. Ely, D. Murphy, J. Seubert, J. Bell, and D. Kuang, "Expected Performance of the Deep Space Atomic Clock Mission," in *AAS/AIAA Space Flight Mechanics Meeting*, 2014.
23. J.D. Prestage, S. Chung, T. Le, L. Lim, and L. Maleki, "Liter sized ion clock with 10^{-15} stability," Proc. Of the joint IEEE IFCS and PTTI, Vancouver, BC, Canada, pp 472-476 (2005).
24. J. D. Prestage and G. L. Weaver, "Atomic Clocks and Oscillators for Deep-Space Navigation and Radio Science," *Proc. IEEE*, vol. 95, no. 11, pp. 2235–2247, Nov. 2007.
25. T. A. Ely, J. Seubert, and J. Bell, "Advancing Navigation, Timing, and Science with the Deep-Space Atomic Clock," in *Space Operations: Innovations, Inventions, and Discoveries*, American Institute of Aeronautics and Astronautics, Inc., 2015, pp. 105–138.
26. R.L. Tjoelker, et al., "Deep Space Atomic Clock (DSAC) for a NASA Technology Demonstration Mission," IEEE Trans. On Ultrasonics, Ferroelectrics, and Frequency Control 63, pp. 1034-1043 (2016).
27. T.A. Ely, E.A. Burt, J.D. Prestage, J.M. Seubert, and R.L. Tjoelker, "Using the Deep Space Atomic Clock for Navigation and Science," IEEE Trans. On Ultrasonics, Ferroelectrics, and Frequency Control 55, pp. 950-961 (2018).
28. J.D. Prestage, G.J. Dick, and L. Maleki, "New ion trap for frequency standard applications," J. Appl. Phys. 66, pp. 1013-1017 (1989).

29. J.D. Prestage, R. L. Tjoelker, and L. Maleki, “Higher pole linear traps for atomic clock applications,” Proceedings of the 1999 Joint European Frequency and Time Forum and IEEE International Frequency Control Symposium, pp. 121-124 (1999).
30. R.H. Dicke, “The effect of collisions upon the Doppler width of spectral lines,” Phys. Rev. **89**, 472 (1953).
31. D. Enzer, W. Diener, D. Murphy, S. Rao, and R.L. Tjoelker, “Drifts and Environmental Disturbances in Atomic Clock Subsystem: Quantifying Local Oscillator, Control Loop, & Ion Resonance Interactions,” IEEE Trans. On Ultrasonics, Ferroelectrics, and Frequency Control 64, pp. 623-633 (2017).
32. S.K. Chung, J.D. Prestage, and R.L. Tjoelker, “Buffer Gas Experiments in Mercury (Hg+) Ion Clock,” Proc. of the IEEE International Frequency Control Symposium, pp. 130-133 (2004).
33. L. Yi, S. Taghavi-Larigani, E.A. Burt, and R.L. Tjoelker, “Progress towards a dual-isotope trapped mercury ion atomic clock: further studies of background gas collision shifts,” Proc. of the 2012 IEEE International Frequency Control Symposium, pp. 1-5 (2012).
34. D.A. Howe, D.W. Allan, and J.A. Barnes, “Properties of signal sources and measurement methods,” Proceedings of the 35th Annual Symposium on Frequency Control, pp. 1-47 (1981).
35. G. J. Dick, “Local oscillator induced instabilities in trapped ion frequency standards,” in Proc. 19th Precise Time and Time Interval Symp., 1987, pp. 133–147.
36. K. M. Larson and J. Levine, "Time transfer using the phase of the GPS carrier," Proceedings of the 1998 IEEE International Frequency Control Symposium (Cat. No.98CH36165), Pasadena, CA, USA, 1998, pp. 292-297
37. K.M. Larson, N. Ashby, C. Hackman, and W. Bertiger, “An assessment of relativistic effects for low earth orbiters: the GRACE satellites,” Metrologia 44, pp. 484-490 (2007).
38. J.D. Prestage, R.L. Tjoelker, G.J. Dick, and L. Maleki, “Doppler sideband spectra for ions in a linear trap,” Proc. of the IEEE International Frequency Control Symposium, pp. 148-154 (1993).
39. R.L. Tjoelker, J.D. Prestage, G.J. Dick, L. Maleki, “Long term stability of Hg+ trapped ion frequency standards,” Proceedings of the 1993 IEEE International Frequency Control Symposium, pp. 132-138 (1993).
40. E.A. Burt and R.L. Tjoelker, “Prospects for ultra-stable timikeeping with sealed vacuum operation in multi-pole linear ion trap standards,” Proc. Of the 39th annual Precise Time and Time Interval Systems and Applications Meeting, pp. 309-316 (2008).
41. Gong Lee Shen, “The pumping of methane by an ionization assisted Zr/Al getter pump,” J. Vac. Sci. Technol. A 5, pp. 2580-2583 (1987).
42. Note that variations in trace gas partial pressure due to temperature-driven outgassing rates would already have been absorbed into the overall temperature effect.
43. A. Konradi, G.D. Badhwar, and L.A. Braby, “Recent space shuttle observations of the South Atlantic Anomaly and the radiation belt models,” Adv. Space Res. 14, pp. 911-921 (1994).
44. G. P. Ginet, D. Madden, B. K. Dichter and D. H. Brautigam, "Energetic Proton Maps for the South Atlantic Anomaly," 2007 IEEE Radiation Effects Data Workshop, Honolulu, HI, 2007, pp. 1-8.
45. R.L. Jerde, L.E. Peterson, and W. Stein, “Effects of high energy radiations on noise pulses from photomultiplier tubes,” Rev. Sci. Inst. **38**, 1387 (1967).